ELSEVIER

Journal of Electron Spectroscopy and Related Phenomena 113 (2001) 241–251

JOURNAL OF ELECTRON SPECTROSCOPY and Related Phenomena

www.elsevier.nl/locate/elspec

The photoemission Fermi edge as a sample thermometer?

J. Kröger[a,*], T. Greber[b], T.J. Kreutz[b], J. Osterwalder[b]

[a]*Christian-Albrechts-Universität zu Kiel, Institut für Experimentelle und Angewandte Physik, Leibnizstrasse 19, D-24098 Kiel, Germany*
[b]*Physik-Institut der Universität Zürich, Winterthurerstrasse 190, 8057, Zürich, Switzerland*

Received 14 February 2000; received in revised form 18 December 2000; accepted 20 December 2000

Abstract

In angle-resolved photoemission from single-crystal samples, the shape of the Fermi edge can be severely distorted by electronic bands crossing the Fermi energy. Analysing temperature-dependent angle-resolved photoemission data from the (111) surface of nickel metal, we explored how far the spectral background below such bands can be described by a Fermi–Dirac distribution function and, intimately connected with this discussion, how far we can deduce the temperature of the sample from this background. For this purpose, we present a fitting procedure that is applicable to angle- and energy-resolved photoemission data sets which permits one to selectively remove band transitions from such data and to extract this background in a reliable fashion. The sample temperature can be reasonably, but not quantitatively, determined by this procedure.

Keywords: Angle-resolved photoemission; Photoelectron emission; Surface electronic phenomena; Nickel; Low index single-crystal surface

1. Introduction

In principle, the width of the Fermi edge in photoemission could be used in order to measure the temperature of a sample surface. There are experimental situations where more common means for temperature measurement are not applicable or not accurate enough. For instance, sample transfer in ultrahigh vacuum equipment excludes the attachment of a thermocouple to the sample. Infrared pyrometer readings depend strongly on the emissivity of the surface, which is often not well known and which may change due to sample treatments in the course of an experiment. More importantly, in the presence of temperature gradients on the sample, or if fast or transient temperature changes need to be monitored, conventional methods for temperature measurement will not work.

Angle-resolved photoelectron spectroscopy is by now a well-established technique for the analysis of crystal surfaces. Using X-ray excitation, the surface structure can be characterized by X-ray photoelectron diffraction (XPD) [1,2] in addition to the more standard chemical analysis by X-ray photoelectron spectroscopy [3]. Angle-resolved ultraviolet photoelectron spectroscopy (ARUPS) is a direct probe for electronic band dispersion [4,5] and momentum distribution, especially for the Fermi surface [6,7]. A review of various combined applications of these photoelectric techniques has been published recently by Aebi et al. [8]. Recent improvements in energy and angular resolution have also opened the path to

*Corresponding author. Tel.: +49-431-880-3966; fax: +49-431-880-1685.
E-mail address: kroeger@physik.uni-kiel.de (J. Kröger).

0368-2048/01/$ – see front matter
PII: S0368-2048(01)00231-6

study thermal effects on electronic degrees of freedom [9,10]. By combining such studies with temperature-dependent structural information from X-ray photoelectron diffraction experiments, one can learn how electronic and nuclear degrees of freedom are coupled, a topic that is at the very base of solid state and surface physics.

For such experiments, a precise knowledge of the surface temperature at the measurement spot and time is needed. It would be most attractive if the temperature could be extracted from the photoemission signal directly. Temperature-dependent changes in photoemission spectra have been demonstrated. In aluminum, for instance, the energy separation of plasmon loss peaks depends on the temperature through the thermal expansion of the lattice and the associated change in electron density [11]. If calibrated properly, Debye–Waller effects in photoelectron diffraction signals could be used [12]. However, the spectral feature that is most directly related to the sample temperature is the width of the Fermi edge in high-resolution ARUPS. Unfortunately, the shape of the Fermi edge is not exclusively determined by the Fermi–Dirac distribution function, but is also determined by the density of states of the sample [13], by final state effects [14,15], by many-body interactions [16–18] and by the resolution of the spectrometer. It can be severely perturbed by band transitions, which usually happen in the region of interest in such studies. One may hope that the spectral intensity forming the smooth background underneath the band transitions is produced by electrons that have undergone enough uncorrelated scattering processes that they are essentially Fermi–Dirac-distributed. In this paper, we present a fitting routine that selectively removes the band-transition signals from photoemission data and that can extract reasonable, although not quantitatively correct, temperature values from ARUPS data in such situations. The examples shown are restricted to experimental data from clean Ni(111) recorded at various temperatures.

2. Fitting procedure

The experimental setup and the complete data set used for this study are given in detail in Ref. [10,19] and, hence, we restrict ourselves to describing the fitting algorithm used for extracting the sample temperature. At the very beginning of our fitting routine is a two-dimensional data set such as the one displayed in Fig. 1. It contains a collection of photoelectron energy distribution curves, which were obtained for a series of polar angles by illuminating the clean (111) surface of Ni with HeIα (21.21 eV) radiation. As one can see, the electron-binding energy, E_B, is plotted versus the polar angle, θ, and the intensities of all energy distribution curves are transformed into a linear gray-scale pattern. The chosen azimuthal orientation of the crystal is 67° off the [$\bar{1}$10] direction and 23° off [$\bar{1}\bar{1}$2] (see Ref. [10,19]). The polar angle, θ, varies from 0 to 76° in steps of 1°; the electron-binding energy values range from $E_B = 550$ meV to $E_B = -350$ meV in steps of

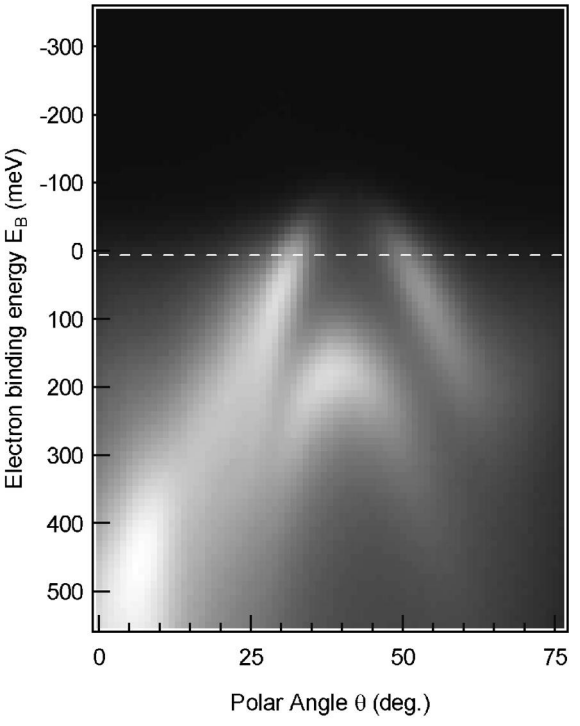

Fig. 1. A typical, polar angle-scanned collection of energy-distribution curves where the electron-binding energy is plotted versus the polar angle. The measured intensity is turned into a linear gray-scale pattern. In this particular data set, taken at room temperature, the exchange-split minority and majority d-bands of Ni(111) at room temperature are presented. The data were taken on an azimuth ϕ 67° off [$\bar{1}$10] and 23° off [$\bar{1}\bar{1}$2] (From Ref. [10]).

10 meV. Thus, the Fermi level (E_F) is crossed. The corresponding decrease in intensity beyond E_F is obvious. The bright contours in the center of Fig. 1 arise from emission from near the top of the minority and majority d-bands that are exchange split at room temperature [19]. The first step of the fitting algorithm consists of successively taking all angular distribution curves, i.e., horizontal sections in the data set of Fig. 1, for energies slightly below E_F up to the maximum kinetic energy of the photoelectrons. In our particular case, this energy interval ranges from $E_B = 40$ meV to $E_B = -350$ meV. We do not extend the fitting interval to higher binding energies in order to avoid intensities from the majority d↑ band (Fig. 1). An example of an angular distribution curve that was recorded precisely at E_F is shown in Fig. 2 (experimental data are displayed as crosses). The curve exhibits two prominent contributions, both associated with the Fermi level crossing of the minority d-band (d↓), as well as a weak shoulder that is due to sp-band emission of both spin channels (sp↑, sp↓) [19]. These experimental data are now approximated by a fitting function that is the superposition of three Gaussians (displayed as open diamonds) matching the dominant peaks and a suitable background (represented as open circles). Note that the fitting takes place on the angular interval and, consequently, a more complex line shape of the direct transition lines can be avoided. The latter would be needed if the fitting was performed on the energy scale [13]. For this particular data set, we found that the background fell off on either side of the band signals and that it could be approximated by a parabola. The fitting of the approximating function to the experimental data has been performed over the entire angle interval using a least-squares algorithm (see Fig. 2). The specific choice of a parabola as an angular background function is purely pragmatic, and it applies for this particular k-space region. Below, we will show a different data set where another shape of the background (linear) proved necessary for good fits to be obtained. The physical origin of the observed angular background will be discussed in the third section of this publication.

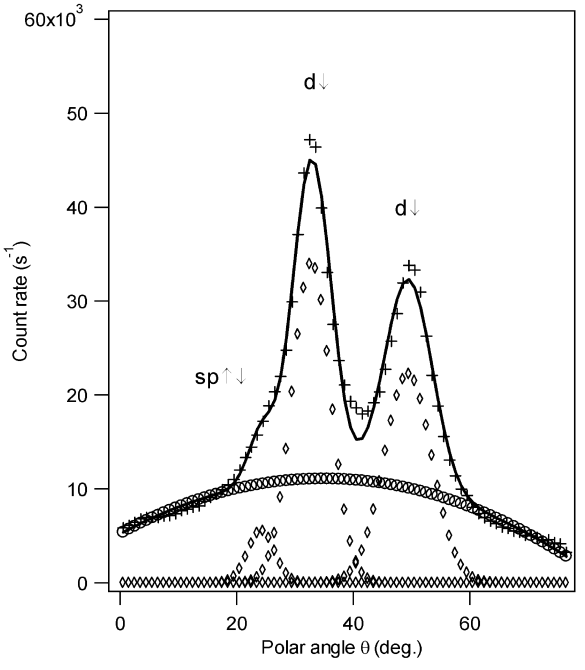

Fig. 2. Angular distribution curve (ADC) taken at the Fermi level. The crosses represent raw data of Fig. 1; the diamonds and circles display the components of the used fitting function, i.e., three Gaussians for the band transitions (sp↑↓ and d↓) and a parabola matching the background, respectively. The fitting function itself is displayed by a solid line. The fitting was performed on the entire angle interval.

From this procedure, which was repeated for energies between 40 and −350 meV, several fitting parameters were obtained: a very precise tracing of the band dispersion is provided by the angular positions of the Gaussians (Fig. 3a) even for energies above E_F [20]; the angular widths (Fig. 3b) of these Gaussians are related through the dispersion relation to the linewidths in the energy spectra that contain information on the lifetimes of the photohole and the photoelectron [21,22]. Note that the exact tracing of the positions and the determination of the angular widths become difficult when the Boltzmann tail of the Fermi–Dirac distribution function dives below the constant background level, which is produced essentially by the polychromatic background in the UV radiation and by detector dark counts. This happens at about $5k_BT$ (i.e. ≈ 125 meV for this data set) in our spectrometer [10]. Thus, Fig. 3 only displays data that could be extracted unambiguously. The solid and open squares in Fig. 3a demonstrate well that the top of the minority d band is sampled in this $\boldsymbol{k}$ region [10].

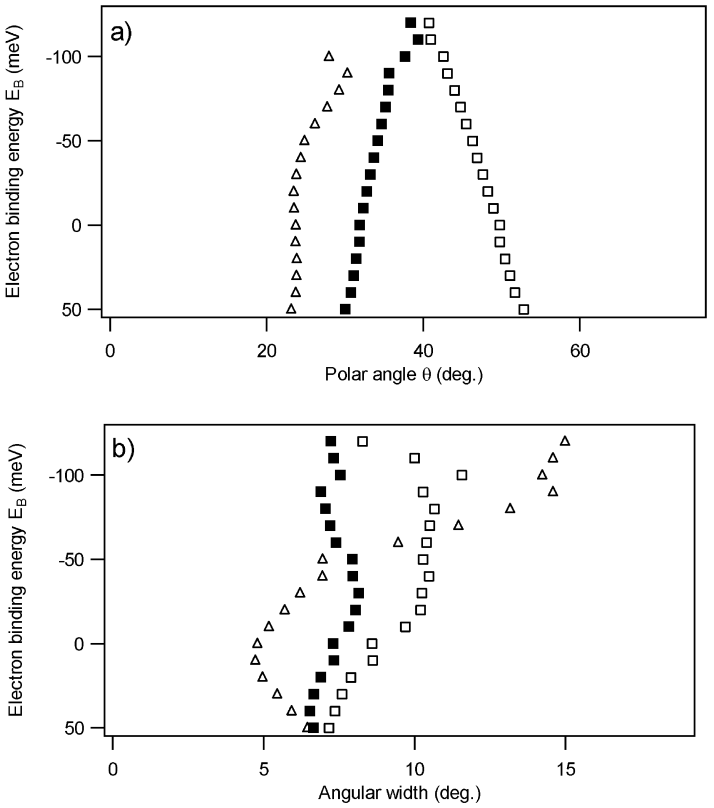

Fig. 3. Extracted fit parameters after approximating the ADCs for energy binding values, 40 meV $\geq E_B \geq -125$ meV. (a) Tracing of the positions of the Gaussians, i.e., the dispersion of the d- and sp-bands [displayed as full (hollow) squares and hollow triangles, respectively]; (b) the corresponding angular widths of the Gaussians.

The background function (shown as circles in Fig. 2) is the specific target of the present analysis: it represents a smooth, slowly varying spectral feature that is not perturbed by band transitions and from which we hope to extract the sample temperature. This is the next step of the fitting algorithm: for each angular distribution curve between 40 and -125 meV, only the parabolic background is retained after the fitting and compiled into another energy versus angle plot. In Fig. 4, we have visualized the resulting background distribution of the raw data of Fig. 1. In the next step, we looked at the energy dependence of this background for each angle between 0 and 76° and approximated it using the following function:

$$g(B, S, T, E_F; E) = B + S \times f(T, E_F; E) \quad (1)$$

with

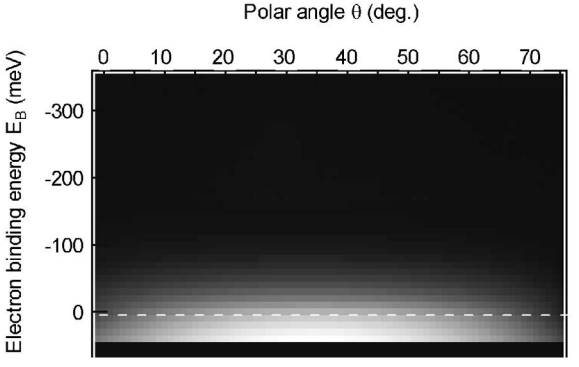

Fig. 4. Angle-scanned background of the data given in Fig. 1. Only the parabolas from the fitting procedure demonstrated in Fig. 2 are retained for each energy level between 40 and -125 meV and their intensities are plotted in a linear gray-scale.

$$f(T, E_F; E) = [\exp(\beta(E - E_F)) + 1]^{-1} \quad (2)$$

the Fermi–Dirac distribution function [$\beta = (k_B T)^{-1}$]; notice that $E - E_F = -E_B$. There are four fitting parameters: B is the above-mentioned constant background and S matches the step height of the Fermi edge; T is the sample temperature (see also Fig. 5a for an explanation of the fitting parameters). Note that we did not include the broadening of the Fermi–Dirac distribution function due to the energy resolution of the analyzer. For the energy resolution of the present data ($\Delta E = 40$ meV) and the temperature range we are interested in, the convolution of the Fermi–Dirac function with a Gaussian representing the instrumental resolution does not affect the value of the temperature seriously. This fact will be exposed in more detail in the next section. Since we know the value of E_F precisely from experiments on polycrystalline Ag (see inset in Fig. 5a), we leave this parameter fixed and only vary the remaining parameters. The fitting is performed via a least-squares algorithm on the energy interval starting from -125 meV and extending up to the Fermi energy. Fig. 5a shows an example of such a fit for the polar angle $\theta = 41°$, which is at the apex of the d↓-band. This figure also contains the raw data (represented as crosses) in order to demonstrate the degree to which the Fermi edge can be perturbed by band transitions. The Fermi edge seems to be shifted towards negative binding energies, i.e., to where the perturbing transition lies. The background function, however, appears to be Fermi–Dirac-distributed around the proper Fermi level.

The inset of Fig. 5a shows the result of the fitting of the Fermi–Dirac distribution function to the Fermi edge of polycrystalline Ag, which was recorded at room temperature. As discussed in the next section, this serves to give an idea of the general accuracy of our fitting routine. For each polar angle θ, we now extract the temperature T_{fit} from the fitting function g and plot it versus θ. The result is displayed in Fig. 6. In the center of the interval, there is a plateau region where the fit values fall close to room temperature, which was the sample temperature for this data set. At the boundaries of the angle interval, the obtained fit values rise to unrealistically high temperature values. In Fig. 5b, we demonstrate, by showing an electron energy distribution curve recorded at a polar angle $\theta = 0°$ that is sufficiently far from the direct transition lines, that the background, for a given angle, cannot be interpreted as a constant times a Fermi–Dirac distribution function with a reasonable temperature. The raw data (crosses) as well as the fitted Fermi edge (full line) show a slightly broader tail compared to the Fermi edge taken from Fig. 5a (displayed as circles). Thus, one must conclude that, since the Fermi edge of the EDC shown in Fig. 5b is not distorted by direct transitions, the resulting higher temperature values are intrinsic to the data and not an artefact of our fitting routine.

3. Results and discussion

We have seen that the precise dispersion of the bands crossing the Fermi level and the angular widths of the transition lines can be extracted by means of the present fitting routine (see Fig. 3). Now we focus on the meaning and the reliability of the fitted temperature values $T_{fit}(\theta)$. Before going into detail, a few words should be dedicated to the general accuracy of our fitting procedure: the inset of Fig. 5a shows the result of the application of the fitting algorithm to the Fermi edge of polycrystalline Ag at room temperature. From these data, no perturbing band transitions had to be subtracted, and since Ag has a fairly constant density of states near E_F, the intensity should be purely Fermi–Dirac-distributed. Using a fitting interval from $E_B \approx -450$ meV to the known Fermi energy, we obtained $T_{Sample} = 328$ K [see Eq. (3) for an explanation of T_{Sample}] for a sample temperature that differed slightly from room temperature.

The $T_{fit}(\theta)$ curve obtained from the data of Fig. 1 is shown in Fig. 6. At both ends of the angle interval, the fitting parameter T_{fit} takes unreasonably high values. Nevertheless, there is a region of $T_{fit}(\theta)$, extending from ≈ 20 to $\approx 60°$, where the values of T_{fit} vary slowly and fall into a reasonable temperature range. The shaded area marks the measured sample temperature. Note that the precision of our temperature measurement is limited: in the photoemission measurement position, our transferrable sample holders are pressed onto a thermal contact containing a Cr/NiCr thermocouple. As a first guess

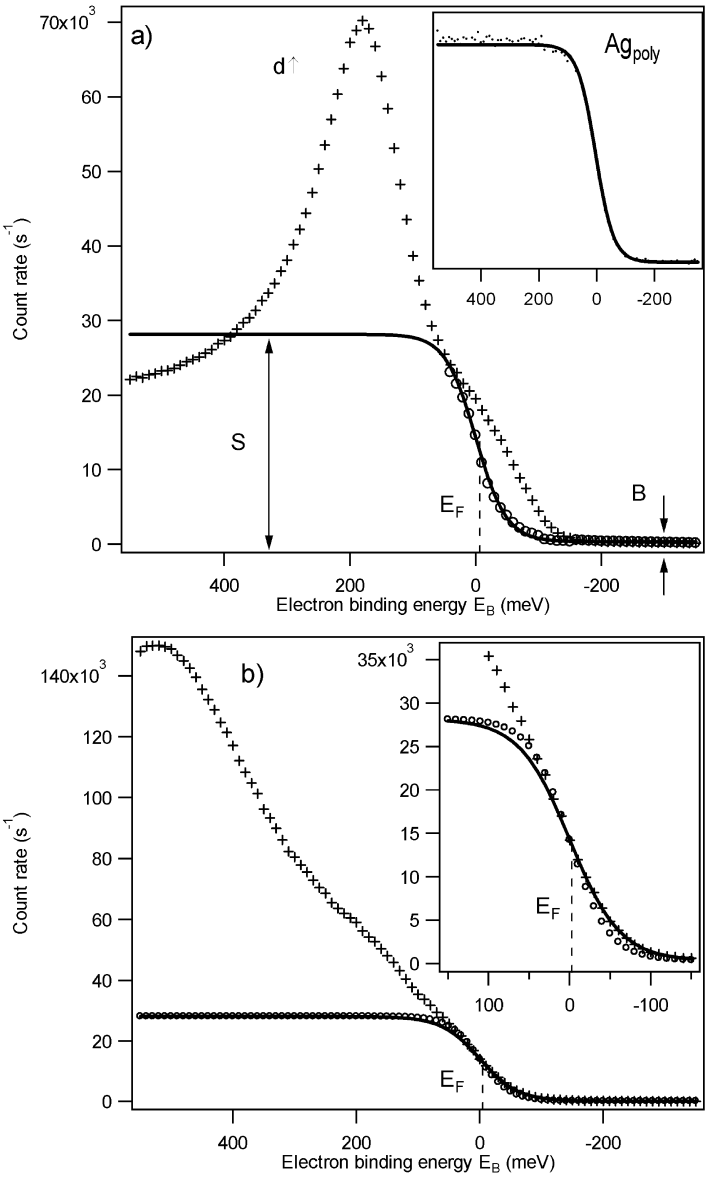

Fig. 5. (a) Energy dependence of the angle-scanned background of Fig. 4. The energy distribution curve shown was taken at the polar angle $\theta = 41°$. Raw data are represented by crosses; the circles represent data from the angle-scanned background and the full line is the graph of the fitting function [see Eq. (2) in the text]. The fitting parameters B (offset), S (step height) and E_F (which is fixed, see text) are indicated. The inset shows a Fermi edge measured on a clean polycrystalline Ag sample at room temperature. (b) Corresponding data taken at an angle far from the direct transition lines. The raw energy distribution curve (displayed as crosses) was recorded at the polar angle $\theta = 0°$. Also included is the fitted Fermi edge for these raw data (full line) and the fitted Fermi edge from (a) (circles). The inset clearly shows a deviation between these two Fermi edges and thus proves that a broadening of the Fermi edge of the raw data at $\theta = 0°$ is inherent in the raw data.

of the temperature of the crystal obtained from the fits, we take the whole angle interval (0 to 76°) to calculate the arithmetic mean $\langle T_{\mathrm{fit}} \rangle$ and its mean deviation $\Delta(\langle T_{\mathrm{fit}} \rangle)$. The results for the room-temperature data are $\langle T_{\mathrm{fit}} \rangle = 307\,\mathrm{K}$ and $\Delta(\langle T_{\mathrm{fit}} \rangle) = 4\,\mathrm{K}$. Fig. 7 demonstrates that the fitting parameter T_{fit} displays

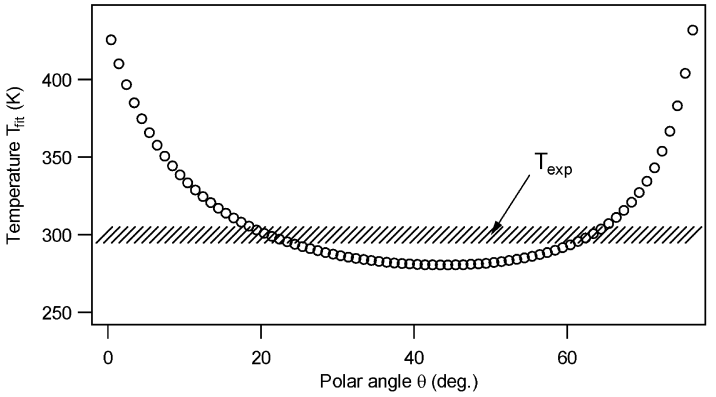

Fig. 6. Behavior of the fitted temperature value, T_{fit}, as a function of the polar angle. The experimental temperature $T_{exp} = (300 \pm 5)$ K is also displayed.

similar behavior for all temperatures investigated, i.e., bad values at the boundaries of the angle interval and a plateau region in between. In Table 1, we compare the fitted temperature values to the experimentally determined value T_{exp}. In doing so, we took the arithmetic mean values $\langle T_{fit} \rangle$ obtained from the $T_{fit}(\theta)$ curves and removed the contribution to the experimental broadening due to the spectrometer resolution, ΔE, via

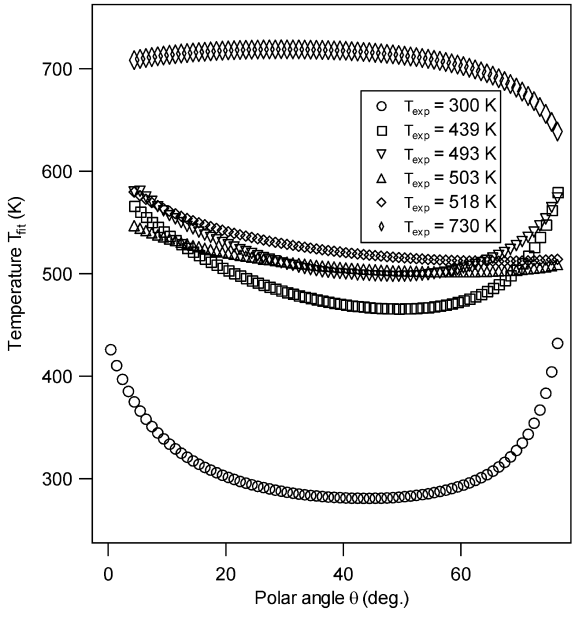

Fig. 7. Fitted temperature curves $T_{fit}(\theta)$ as in Fig. 6 for analogous data sets measured at various temperatures, T_{exp}.

$$T_{Sample} = \sqrt{\langle T_{fit} \rangle^2 - \left(\frac{\Delta E}{4k_B} \right)^2}. \quad (3)$$

This procedure was introduced by Kreutz et al. [19], who showed that the convolution of the Fermi–Dirac function with a Gaussian of width ΔE results in a Fermi–Dirac-like function with an increased effective temperature, which equals $\langle T_{fit} \rangle$ in our present case. As can be deduced from Table 1, the influence of the energy resolution of the spectrometer ($\Delta E =$ 40 meV) is small. In principle, a finite angular resolution of the instrument leads to a broadening of the observed direct transition lines. Since the angular resolution of our instrument was set to $\approx 2^\circ$ full width at half maximum and the observed angular width of the direct transition lines is about 10°, one

Table 1
Comparison of three temperature values: T_{exp}, as measured experimentally by means of a thermocouple, $\langle T_{fit} \rangle$, extracted as the arithmetic mean value of $T_{fit}(\theta)$ from the fitting procedure applied to polar scan data such as that shown in Fig. 1, and T_{Sample}, which is the effective temperature that takes into account the convolution of the Fermi–Dirac distribution function with a Gaussian representing the broadening due to the finite resolution of the energy analyser (see also Eq. (3) in the text)

$\langle T_{fit} \rangle$ (K)	T_{Sample} (K)	T_{exp} (K)
307±4	≈284	300±5
495±4	≈481	439±13
521±3	≈508	493±12
512±1	≈499	503±12
528±2	≈515	518±12
706±2	≈696	730±27

should not expect a significant impact of the instrument's resolution on the fitting results. The sample temperature values obtained from our fitting algorithm and those from thermocouple readings are in reasonable, although not perfect, agreement, if we take the mean value $\langle T_{\mathrm{fit}} \rangle$ over the entire angle interval. If we take only the plateau region, where $T_{\mathrm{fit}}(\theta)$ is more or less stable, the sample temperature is significantly underestimated (see Fig. 6). It is worth mentioning that the unreasonable increase in the fitted temperature value at the boundary of the angle interval is not an artefact of our fitting routine and especially of the choice of the background function. Fig. 5b demonstrates clearly that the broadening of the Fermi edge is a property of the raw data: the inset of Fig. 5b shows the raw data near the Fermi energy, E_{F} at $\theta = 0°$ (displayed as crosses), the fit of the Fermi edge (solid line) and the fitted Fermi edge from Fig. 5a, i.e., from the background data at $\theta = 41°$. Obviously, the Fermi edge of the raw data at $\theta = 0°$ is broader than the fitted Fermi edge at $\theta = 41°$, leading to the above-stated higher temperature value. Since, at $\theta = 0°$, one is sufficiently far away from the distorting band transitions, one must deduce that the broadening of the Fermi edge is inherent in the raw data. A similar reasoning applies to the other boundary of the angle interval ($\theta = 76°$).

In order to test the general applicability of our fitting procedure, we analysed another data set obtained from Ni(111) [19] where the emission geometry and the band dispersion were different. In Fig. 8, we display azimuthal angle-scanned energy-distribution curves from Ni(111) measured at ≈ 370 K and at a fixed polar angle of $\theta = 78°$. The azimuth is measured from the [$\bar{1}$12] direction. The dispersing features have been identified as exchange-split sp-bands [19]. The energy-distribution curves range from $E_{\mathrm{B}} = 600$ meV to $E_{\mathrm{B}} = -300$ meV in steps of 5 meV and were recorded every 0.43° in ϕ. The fitting procedure was applied using four Gaussians matching the band transitions and a background which can be well approximated by a linear function in angle in this case. Again, the use of this linear function for the angular dependence of the background results from a purely pragmatic point of view, i.e., the linear function leads to good fits throughout the whole energy- and angle scale. The

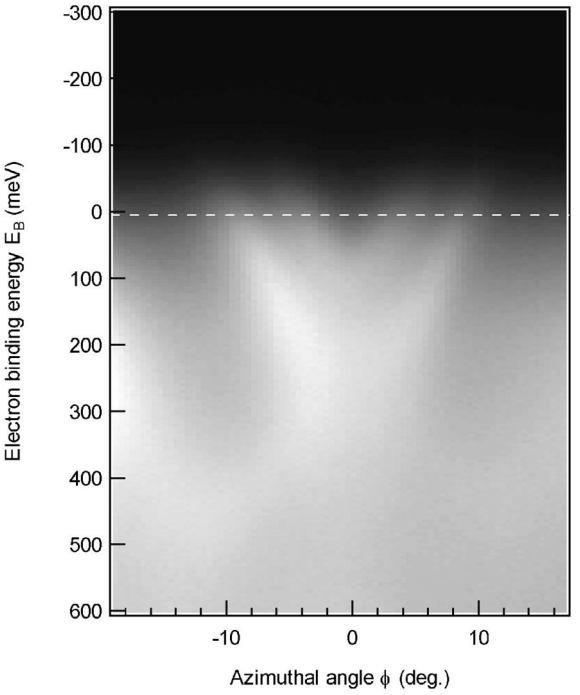

Fig. 8. Azimuthal angle-scanned collection of energy-distribution curves from Ni(111), measured at room temperature and taken at a fixed polar angle $\theta = 78°$. In this $\boldsymbol{k}$-region, the dispersion of the exchange-split sp-bands can be observed [19].

fitting takes place on the entire angle interval. Fig. 9a shows the fitting result for the angular distribution curve extracted at E_{F}. In analogy to Fig. 2, the superposition of the four Gaussians and the straight line is found to produce an excellent fit to the data. In Fig. 9b, we demonstrate the fitting of the Fermi–Dirac distribution function to the angular background function at $\phi = -14°$. Again, the serious perturbation of the Fermi edge by the band transitions is revealed. Finally, Fig. 9c displays T_{fit} as a function of the azimuthal angle. The behavior of this curve is quite different from that of earlier cases. As the angular background happens to be a straight line for each energy value between $E_{\mathrm{B}} = 50$ meV and $E_{\mathrm{B}} = -300$ meV, which is the energy interval for the fitting algorithm, the $T_{\mathrm{fit}}(\phi)$ curve must also be linear. Taking again all angles for the calculation of the arithmetic mean, we obtain $\langle T_{\mathrm{fit}} \rangle = 394$ K, with a mean deviation of $\Delta(\langle T_{\mathrm{fit}} \rangle) = 0.5$ K. This fit value is again in reasonable, but not quantitative, agreement

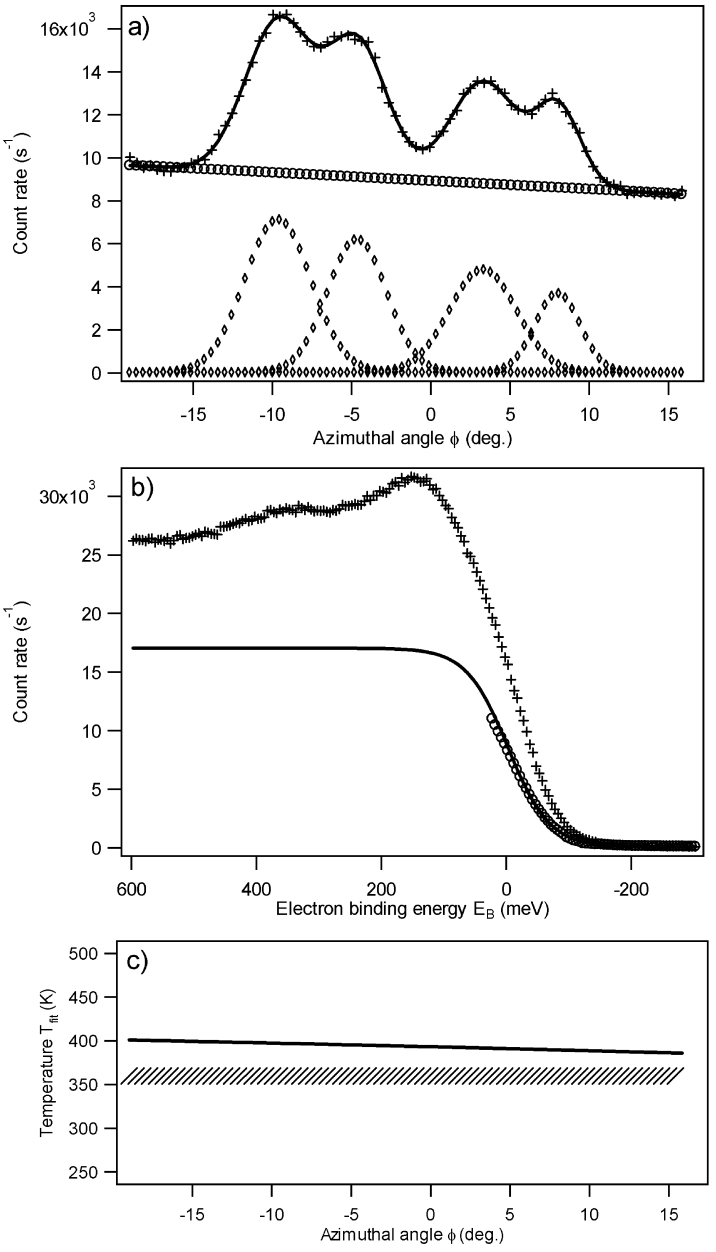

Fig. 9. (a) Angular distribution curve extracted from Fig. 8 at the Fermi level. The data are fitted to four Gaussians and a linear background. (b) Fermi–Dirac fit to the angle-scanned background at an arbitrarily chosen azimuth of $\phi = -14°$ and comparison of the Fermi edge of the raw data (shown as crosses) with the Fermi edge after removal of the direct transition lines (circles). (c) Results for the fitted temperature values, T_{fit}, as a function of ϕ.

with the measured temperature (370 ± 10 K). We applied the fitting routine to yet another data set that measures the bands of Fig. 8 at elevated temperatures. The angular background function could be fitted by a straight line with vanishing slope. We do not show the corresponding images and restrict

Table 2
Same as Table 1, but now the values correspond to the azimuthal angle-scanned collection of energy-distribution curves of Fig. 8 and to a corresponding data set measured at elevated temperature

$\langle T_{fit} \rangle$ (K)	T_{Sample} (K)	T_{exp} (K)
394±0.5	≈377	372±15
619±0	≈608	693±30

ourselves to summarize the obtained data in the second row of Table 2. Next, we wanted to know the physics behind the angular dependence of T_{fit}, which lead us to the question of the physics behind the photoemission background on the angular scale, i.e., in momentum space. Having in mind that our fitted temperature values are reasonably consistent with the experimental thermocouple readings, but do not reproduce these readings quantitatively, one must conclude that, even after removing the band transitions from the investigated spectra, the remaining background cannot be interpreted as a constant times a Fermi–Dirac distribution function with a reasonable temperature. Consequently, we should try to identify contributions to the background photocurrent that deform the Fermi edge. Put more precisely, the angular distribution of this smooth background has to be known for each energy value, since this entity will define the shape of the background Fermi edge at each angle. This question has recently been addressed by Lindroos and Bansil [23], who identified indirect transitions due to photoelectron–electron interaction as an important contribution to the angular spectral background. They did not study the energy- and temperature-dependence of these diffuse intensities. Manghi et al. [17] have shown that many-body interactions in the photohole state are quite important in the case of Ni. Due to the strongly temperature-dependent electronic structure of ferromagnetic Ni [19], this effect could be responsible for a T-dependent redistribution of background intensities. Likewise, indirect transitions due to electron–phonon scattering can contribute in a temperature-dependent fashion to the observed background (see, for instance, Hüfner [5] and references therein). White et al. [24,25] used a simplified $\boldsymbol{k}$-space integration model for phonon-assisted indirect transitions in order to show that the background is maximal in the vicinity of direct transitions. From a comparison of our two different data sets (Fig. 1 and Fig. 8), we can deduce that the angular dependence is sensitive to the dispersion of the investigated bands, i.e., the group velocity of the electrons comes into play. We can only speculate about which contributions dominate the observed background and hope that we stimulate theoretical efforts for a deeper understanding. Finally, let us briefly comment on the applicability of the fitting routine. It should be generally applicable whenever bands with sufficient dispersion are present. The routine demands initial guesses for the number, the positions and the widths of the Gaussians and a suitable form for the angular background function. The fitting routine we introduced in this publication is thus not a black box where data sets of the type shown in Figs. 1 and 8 are the input and the sample temperature is the output.

4. Conclusion

Using polar and azimuthal angle-scanned collections of energy distribution curves from the (111) surface of Ni at various temperatures, we demonstrated that information about the temperature of the sample can be extracted in a reasonable, but not fully quantitative, way. We introduced a fitting algorithm that, in a first step, subtracts the band transitions from the data and, in a second step, fits the Fermi–Dirac distribution function to the remaining background. The resulting temperature values are in reasonable accord with thermocouple readings. At angles far away from band transitions, marked deviations occur that indicate that the remaining background cannot be interpreted as a constant times a Fermi–Dirac distribution function with a realistic temperature value. This reflects the fact that the scattering processes of the photohole and the photoelectron that redistribute photocurrent away from the direct transition lines into the background are energy- and momentum-dependent. With the advance of new, high-resolution electron spectrometers and synchrotron radiation beam lines, this type of two-dimensional data in the form of energy versus angle dispersion plots will be more readily available, and such procedures for extracting peak dispersion, line widths and sample temperature will be highly wel-

come. Moreover, we would like to stimulate more theoretical work characterizing the temperature dependence and the $\boldsymbol{k}$-dependence of spectral functions near the Fermi level.

References

[1] C.S. Fadley, in: R. Bachran (Ed.), Synchrotrone Radiation Research: Advances in Surface Science, Plenum, New York, 1990.
[2] J. Osterwalder, P. Aebi, R. Fasel, D. Naumović, P. Schwaller, T.J. Kreutz, L. Schlapbach, T. Abukawa, S. Kono, Surf. Sci. 331–333 (1995) 1002.
[3] D. Briggs, in: C.R. Brundle, A.D. Baker (Eds.), Analytical Applications of XPS; Electron Spectroscopy: Theory, Techniques and Applications, Vol. 3, Academic Press, New York, 1979.
[4] E.W. Plummer, W. Eberhardt, Adv. Chem. Phys. 49 (1982) 533.
[5] S. Hüfner, in: Photoelectron Spectroscopy, Springer Series in Solid State Sciences 82, Springer, Berlin, 1995.
[6] A. Santoni, L.J. Terminello, F.J. Himpsel, T. Takahashi, Appl. Phys. A 52 (1991) 229.
[7] P. Aebi, J. Osterwalder, R. Fasel, D. Naumović, L. Schlapbach, Surf. Sci. 307–309 (1994) 917.
[8] P. Aebi, R. Fasel, D. Naumović, J. Hayoz, Th. Pillo, M. Bovet, R.G. Agostino, L. Patthey, L. Schlapbach, F.P. Gil, H. Berger, T.J. Kreutz, J. Osterwalder, Surf. Sci. 402–404 (1998) 614.
[9] D. Malterre, M. Grioni, Y. Baer, Adv. Phys. 45 (1996) 299.
[10] T. Greber, T.J. Kreutz, J. Osterwalder, Phys. Rev. Lett. 79 (1997) 4465.
[11] T. Greber, J. Osterwalder, S. Hüfner, L. Schlapbach, Phys. Rev. B 44 (1991) 8958.
[12] R. Trehan, C.S. Fadley, Phys. Rev. B 34 (1986) 6784.
[13] R. Clauberg, K.H. Frank, J.M. Nicholls, B. Reihl, Surf. Sci. 189/190 (1987) 44.
[14] H. Hövel, B. Grimm, M. Pollmann, B. Reihl, Phys. Rev. Lett. 81 (1999) 4608.
[15] R. Joynt, Science 284 (1999) 777.
[16] M. Hengsberger, D. Purdie, P. Segovia, M. Garnier, Y. Baer, Phys. Rev. Lett. 83 (1999) 592.
[17] F. Manghi, V. Bellini, J. Osterwalder, T.J. Kreutz, P. Aebi, C. Arcangeli, Phys. Rev. B 59 (1999) R10409.
[18] T. Valla, A.V. Fedorov, P.D. Johnson, S.L. Hulbert, Phys. Rev. Lett. 83 (1999) 2085.
[19] T.J. Kreutz, T. Greber, P. Aebi, J. Osterwalder, Phys. Rev. B 58 (1998) 1300.
[20] T.J. Kreutz, P. Aebi, J. Osterwalder, Solid State Commun. 96 (1995) 339.
[21] N.V. Smith, P. Thiry, Y. Petroff, Phys. Rev. B 47 (1993) 15476.
[22] J.K. Grepstad, B.J. Slagsvold, I. Bartoš, J. Phys. F 12 (1982) 1679.
[23] M. Lindroos, A. Bansil, Phys. Rev. Lett. 77 (1996) 2985.
[24] R.C. White, C.S. Fadley, M. Sagurton, Z. Hussain, Phys. Rev. B 34 (1986) 5226.
[25] R.C. White, C.S. Fadley, M. Sagurton, P. Roubin, D. Chandesris, J. Lecante, C. Guillot, Z. Hussain, Phys. Rev. B 35 (1987) 1147.